Available online at www.sciencedirect.com
ScienceDirect
Ceramics International 36 (2010) 2047–2053
CERAMICS INTERNATIONAL
www.elsevier.com/locate/ceramint

Synthesis and characterization of TiO_2 nanoparticles

M.M. Viana, V.F. Soares, N.D.S. Mohallem *

Chemistry Department, Federal University of Minas Gerais, Belo Horizonte, MG, CEP: 31270-901, Brazil

Received 15 March 2010; received in revised form 29 March 2010; accepted 28 April 2010
Available online 30 June 2010

Abstract

TiO_2 nanoparticles were synthesized by thermal decomposition of a precipitate obtained from a precursor solution of titanium isopropoxide (IV) and isopropyl alcohol. The as-prepared precipitate was heated at various temperatures and the obtained samples were morphologically, texturally and structurally characterized using TGA–DTA, gas adsorption, SEM, XRD and FTIR. The UV–vis radiation absorption and the photocatalytic activity also were verified. The TiO_2 sample heated at 300 °C shows the best results to be applied as blocker in solar skin protector.

Keywords: A. Calcinations; D. TiO_2; E. Biomedical applications

1. Introduction

TiO_2 is a semiconductor with several applications such as pigments [1], optical filters, antireflection coatings, chemical sensors, catalysts, and sterilization materials [2–6]. This wide range of applications is mainly due to its electronic and structural properties. Other important properties of this material are the high visible spectrum transmittance, high refraction index, chemical stability, and photocatalytic and antimicrobial activity [7–9].

The crystal forms of TiO_2 are anatase, rutile, and brookite. The size and shape of the TiO_2 particles influence the functional properties, specific surface area, amount of defects, phase transition temperatures, and the stability of the different phases [10]. Besides, the optical, textural, and catalytic properties of TiO_2 depend on the crystalline phase, the crystallite size, and the porosity. Therefore, the preparation of nanoparticulate TiO_2 with tailored specific surface area and high porosity for specific applications is of interest due to the new properties expected.

Studies of TiO_2 as a catalyst have shown that rutile is the most efficient phase in sonocatalysis, and anatase in photocatalysis [11,12]. In addition, nanoparticulate TiO_2 can be used in sunscreen lotion to block UV-A and UV-B irradiation. The effectiveness of the solar radiation backscattering depends on the size, shape and phase of TiO_2 nanoparticles [13]. The harmful effects on health due to the use of TiO_2 in sunscreen have been related to the production of free radicals in a photocatalytic mechanism. The TiO_2 in a sunscreen lotion should be photostable to preserve the biological structures of the organisms [14].

As the anatase is more photoactive than rutile phase the free radicals formation is probably higher for anatase phase. Because of this, rutile phase is preferentially used in sunscreen formulations [15]. Furthermore, an anatase–rutile mixture is more effective than each phase separately in photocatalysis, which depends on the electron–hole recombination rate, crystallinity, adsorptive affinity and particles interconnection [16]. The junction of these properties generally guarantees the photocatalysis success that is shown by the Degussa P-25 commercial powder (80% anatase, 25 nm and 20% rutile, 85 nm) [17,18].

In the present work, the effects of heating were correlated with the structural, morphological, and textural properties of the synthesized TiO_2 nanoparticles. The photocatalytic activity and the ultraviolet absorption of the samples also were evaluated.

2. Experimental

2.1. Preparation of TiO_2 powders

Titanium isopropoxide (IV) ($Ti(OCH(CH_3)_2)_4$) 97% (Aldrich) diluted in isopropyl alcohol 99.5% (Merck) was

* Corresponding author. Tel.: +55 31 34095768; fax: +55 31 34095700.
E-mail address: nelcy@ufmg.br (N.D.S. Mohallem).

0272-8842/$36.00
doi:10.1016/j.ceramint.2010.04.006

used as starting solution, where TiO_2 nanoparticles were precipitated on the addition of alkaline distilled water (pH 8). The molar ratio of alkoxide:alcohol:water was fixed at 5:3:1. The as-prepared precipitate was washed using distilled water, centrifuged and heated at temperatures ranging from 200 to 1100 °C.

2.2. Instrumentation

Thermogravimetric–differential thermal analyses (TGA–DTA) were performed in a TA Instruments (SDT 2960). The behaviors of the as-prepared samples were evaluated in air atmosphere from 25 to 1400 °C at 10 °C min^{-1}.

The X-ray patterns obtained in a Rigaku (Geigeflex-3034) diffractometer in the 2θ range 10–80° using Cu Kα radiation (λ = 1.5406 Å) were used to investigate the polymorphic transformations of TiO_2 in the temperature range of 200–1100 °C. The average crystallite size was estimated by Scherrer's equation [19]. The anatase/rutile ratio was determined from the intensity of the XRD peaks and the Spurr and Myers equation [20]:

$$F_R = \frac{1}{1 + 1.26[I_A(1\,0\,1)/I_R(1\,1\,0)]} \quad (1)$$

where F_R is the percentage content of rutile at each temperature, I_A (1 0 1) and I_R (1 1 0) are the integral intensities of (1 0 1) anatase and (1 1 0) rutile, respectively.

Fourier transform infrared spectra (FTIR-Perkin-Elmer, 2838) were recorded in a Spectrum GX FTIR spectrometer in the range of 4000–400 cm^{-1} in pressed KBr pellets.

Scanning electron microscopy (SEM – JEOL JSM, 840) was used to investigate the particle morphologies.

Nitrogen gas adsorption (Autosorb, Quantachrome Nova 1200) was used in the textural analysis of samples degassed at 150 °C for 3 h. The specific surface area and porosity of the samples were determined using the Brunauer–Emmett–Teller (BET) and Barrett–Joyner–Halenda (BJH) methods [21], respectively. Adsorption heat and average particle size were also evaluated.

The ultraviolet and visible absorption of the samples were recorded in a spectrometer (U3010 – Hitachi) between 800 and 200 nm. The samples were dispersed in distilled water with concentration of 5×10^{-4} g L^{-1}, and analyzed in a quartz cell with a 10-mm path length at 25 °C. Photocatalytic tests were performed using an aqueous solution of Drimaren dye (50 mg L^{-1}) containing the different TiO_2 powders. These systems were submitted to UV irradiation treatment in air for 4 h using a UV-C light lamp (Girardi RSE20B, 254 nm) at a power of 15 W.

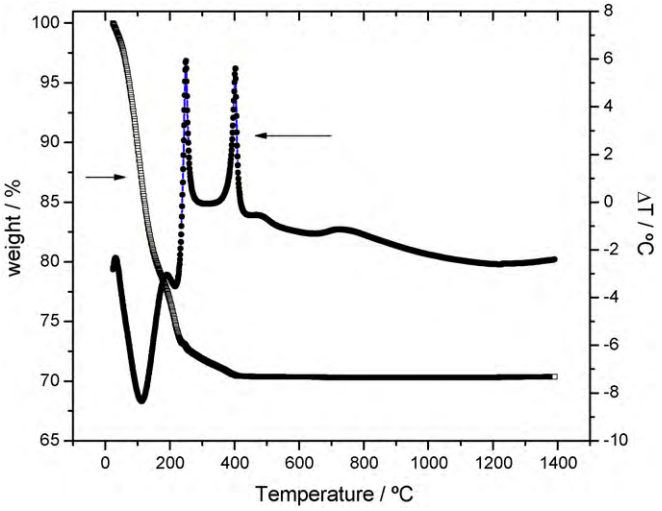

Fig. 1. TGA–DTA curves of as-prepared TiO_2 nanoparticles.

3. Results and discussion

The simultaneous TGA and DTA curves of the as-prepared powders are shown in Fig. 1. The DTA curve exhibits six events, three endothermic and three exothermic. The endothermic peak at 100 °C corresponds to 22% weight loss, related to adsorbed water. The peak at 215 °C is related to a weight loss of 4.5% of structural water. The dehydroxylation and combustion of carbonaceous residues are evidenced by two strong exothermic peaks at ∼250 and ∼400 °C (3.5% total weight loss). These strong peaks mask the crystallization peak of TiO_2, which occurs in the range of 247–327 °C according to Bekkerman et al. [22]. No weight loss is observed above 400 °C associated to the other DTA events. The endothermic event starting around 500 °C, characteristic of densification and/or sintering, is interrupted by a broad exothermic event between 650 and 800 °C related to the anatase–rutile phase transition. This diffuse phase transition may be attributed to heterogeneous nanoparticle sizes [23]. The evolution of the crystallization from amorphous TiO_2 powder can be

Table 1
Textural characteristics of TiO_2 samples as a function of heating temperature (measurements are accurate to within ±7%).

Temperature/°C	S_{BET}/m^2 g^{-1}	C constant	ΔH_{ads}/kJ mol^{-1}	P_{BJH}/%	d_{part}/nm
200	266	37	−7.8	74	6
300	165	86	−8.4	54	9
500	53	76	−8.3	24	30
700	9	41	−7.9	15	160
900	4	37	−7.8	–	350
1100	2	19	−7.4	–	705

S_{BET}, specific surface area; P_{BJH}, porosity relative to meso- and micropores; ΔH_{ads}, adsorption heat; d_{part}, average particle size.

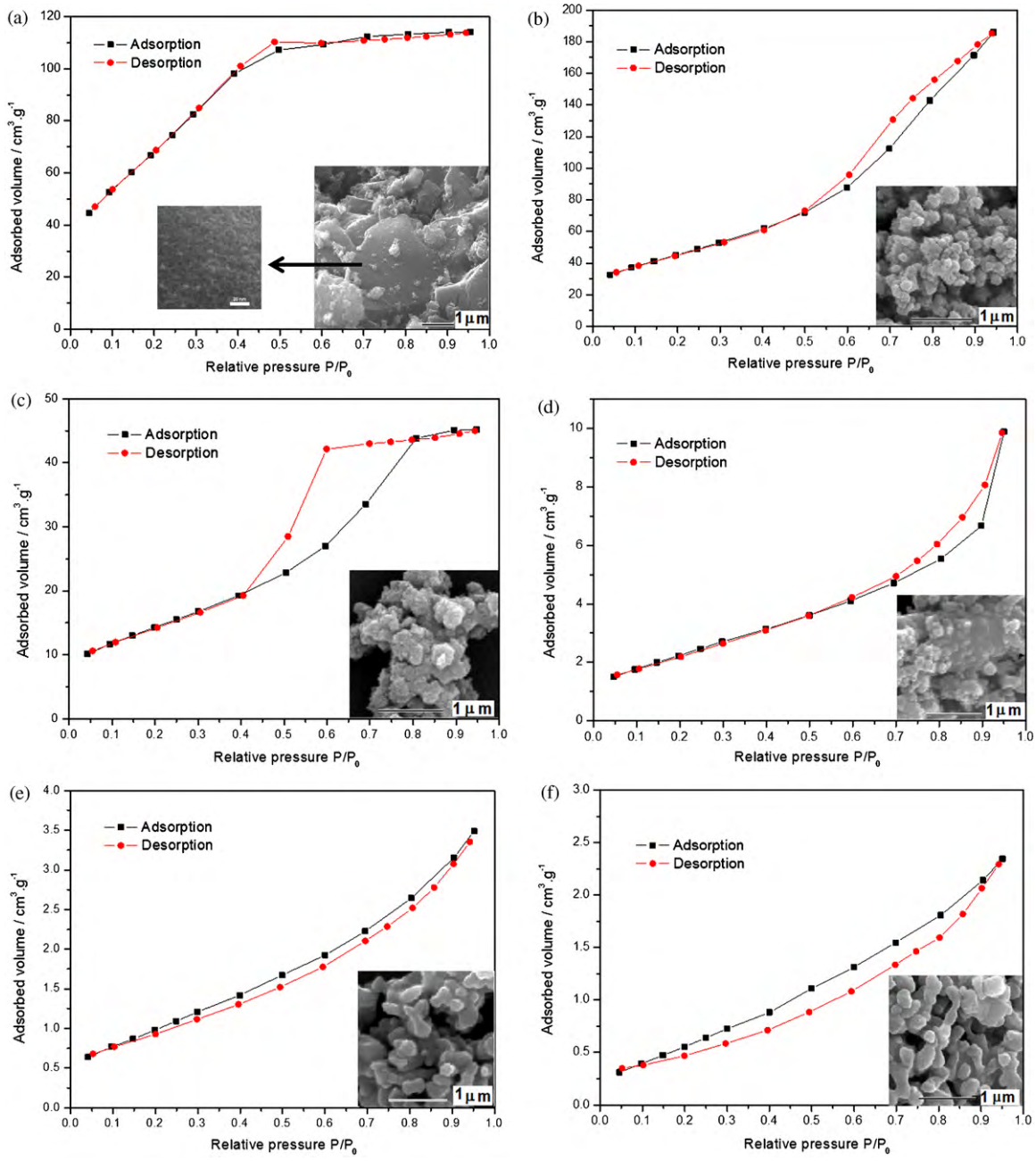

Fig. 2. Adsorption–desorption isotherms of TiO_2 nanoparticles heated at (a) 200 °C, (b) 300 °C, (c) 500 °C, (d) 700 °C, (e) 900 °C, and (f) 1100 °C.

represented as follows:

$$(\text{Amorphous TiO}_2 + \text{adsorbed H}_2\text{O}) \xrightarrow[\text{endo}]{100\,^\circ\text{C}} (\text{Amorphous TiO}_2 + \text{structural H}_2\text{O}) \xrightarrow[\text{endo}]{215\,^\circ\text{C}} \text{Amorphous TiO}_2 \longrightarrow_{\text{exo}} \text{Anatase} \xrightarrow[\text{exo}]{650-800\,^\circ\text{C}} \text{Rutile}$$

Thermal treatment had a great influence on the structural and textural characteristics of the TiO_2 samples, as shown in Table 1. The sample heated at 200 °C shows an isotherm characteristic of materials with micro- and mesopores (Fig. 2a), and it has the largest specific surface area and porosity of 266 $m^2\,g^{-1}$ and 74%, respectively. The porous surface is showed in enlarged image (inset in Fig. 2a). The occurrence of a narrow pore size distribution obtained by the BJH method confirms the micro- and mesopores character (Fig. 3a), with pores measuring between 10 and 50 Å. This sample shows amorphous behavior due to the large amounts of organic residues and water, according to TGA–DTA results. Besides, the low value of *C* constant in the BET equation is due to filling porous by organic compounds, which difficult the adsorbate–adsorbent interaction.

With the liberation of water and organic residues up to 300 °C, it occurs the formation of agglomerates (inset in Fig. 2b) of secondary particles with size between 70 and

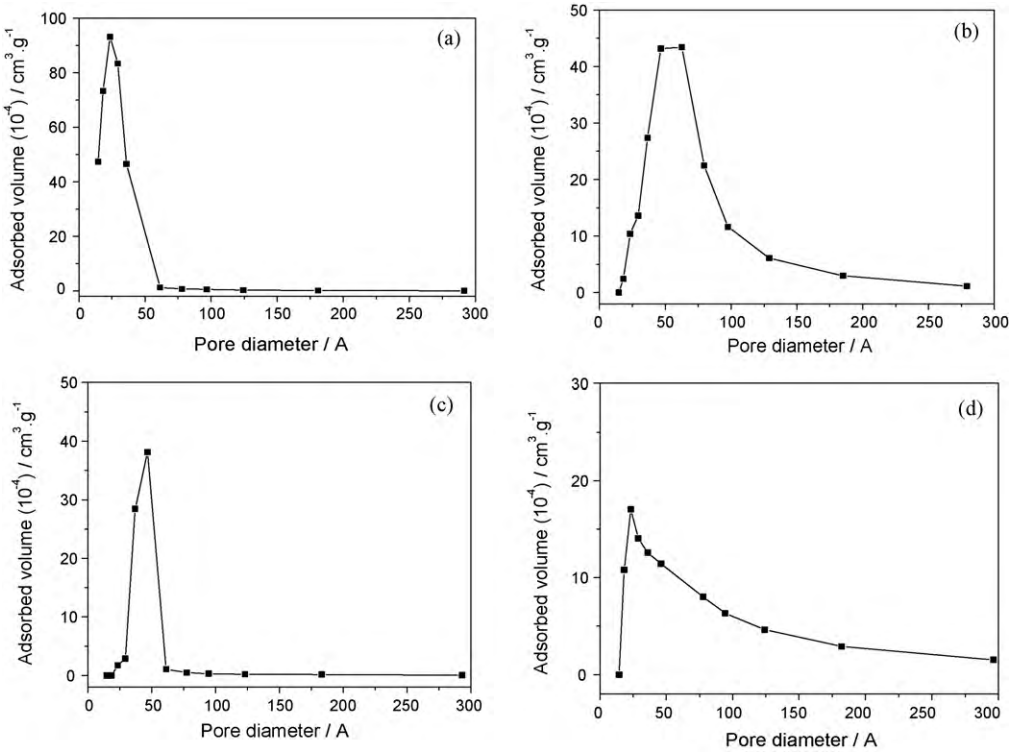

Fig. 3. Pore size distribution of TiO_2 nanoparticles heated at (a) 200 °C, (b) 300 °C, (c) 500 °C and (d) 700 °C.

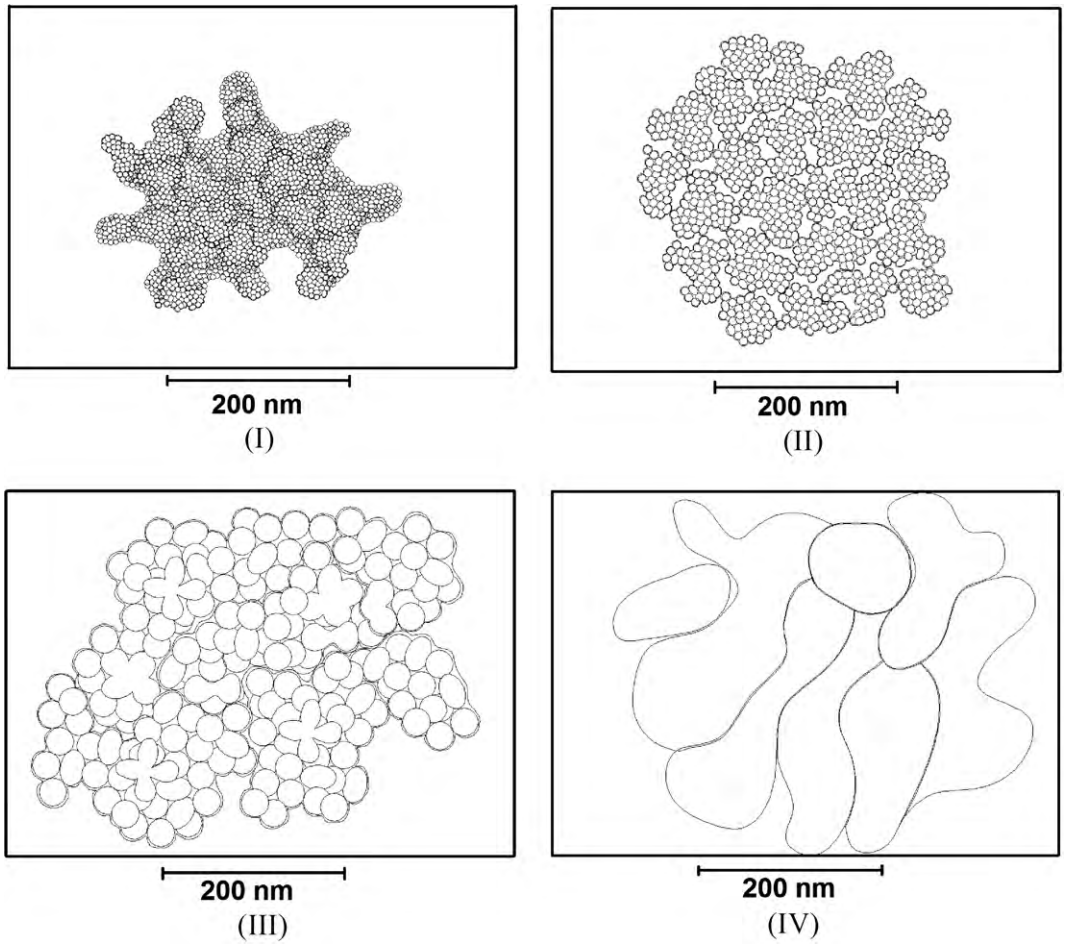

Fig. 4. Scheme of the evolution of the TiO_2 nanoparticles with the thermal treatment temperature.

310 nm (measured by SEM images), which are formed by primary particles with size around 9 nm (measured by XRD and BET method). This sample shows a type IV isotherm (Fig. 2b) according to BDDT classification [21], characteristic of mesoporous materials, with the largest N_2 adsorption value around 195 $cm^3\ g^{-1}$. The specific surface area and porosity diminished to 165 $m^2\ g^{-1}$ and 54%, respectively, and the large pore size distribution obtained by the BJH method shows mesopores measuring between 20 and 300 Å (Fig. 3b). The small pores are formed probably by the agglomeration of the primary nanoparticles and the large mesopores are due to the interstices formed by the agglomeration of the secondary particles (inset in Fig. 3b). A scheme of the evolution of the particles with the thermal treatment is shown in Fig. 4, where data about XRD, gas adsorption and SEM images was taking into account.

XRD patterns of TiO_2 samples heated from 300 to 1100 °C are shown in Fig. 5. The broad diffraction lines of the samples heated at 300 and 500 °C are related to the nanocrystalline anatase phase. The width reduction of the peaks with the temperature is associated to an increase in the crystallite size (Table 2). This result is corroborated by the FTIR shown in Fig. 6. Samples heated at 300 and 500 °C show an absorption band at 1625 cm^{-1} related to the bending mode of the hydroxyl groups of the structural water [24]. This band decreases as the temperature increases. The FTIR stretching vibration of the Ti–O–C band [25] is not present, confirming the TGA–DTA results, which shows no evidence of weight loss event related to residual alkoxy groups. A broad band associated with the characteristic vibrational modes of TiO_2 appears between 880 and 380 cm^{-1} for samples heating at 300 and 500 °C [26].

Table 2
Average crystallite size of TiO_2 samples measured by Scherrer equation.

Temperature/°C	Polymorphic phases	Average crystallite size/nm
300	Anatase	7
500	Anatase	17
700	Anatase (26%)	45
	Rutile (74%)	80
900	Rutile	110
1100	Rutile	165

These combined modes correspond to Ti–O–Ti bond vibrations of the crystalline anatase phase that present a main band at 511.9 cm^{-1} [27,28]. This large band appears mainly due to nanoparticles with large size distribution. The nanoparticle shape and state of aggregation of the nanocrystals can modify the infrared powder spectra inducing shifts, enlargements and superposition of vibrational modes [29].

At 500 °C, the amount of adsorbed gas and the specific surface area decreased to 45 $cm^3\ g^{-1}$ and 53 $m^2\ g^{-1}$, respectively. The sample presents type IV isotherms, characteristic of mesoporous material according to the BDDT classification [21]. The hysteresis loop type H2 according to the IUPAC classification [21] shows a great difficulty of desorption and is characteristic of disordered materials with pore shape not well defined. The narrow pore size distribution that varies between 2 and 60 Å (Fig. 3c) shows that the material is densifying and the large pores are disappearing. The secondary particle sizes decreased to values of about 150–290 nm (measured by SEM images), and the primary particle sizes increased to values of

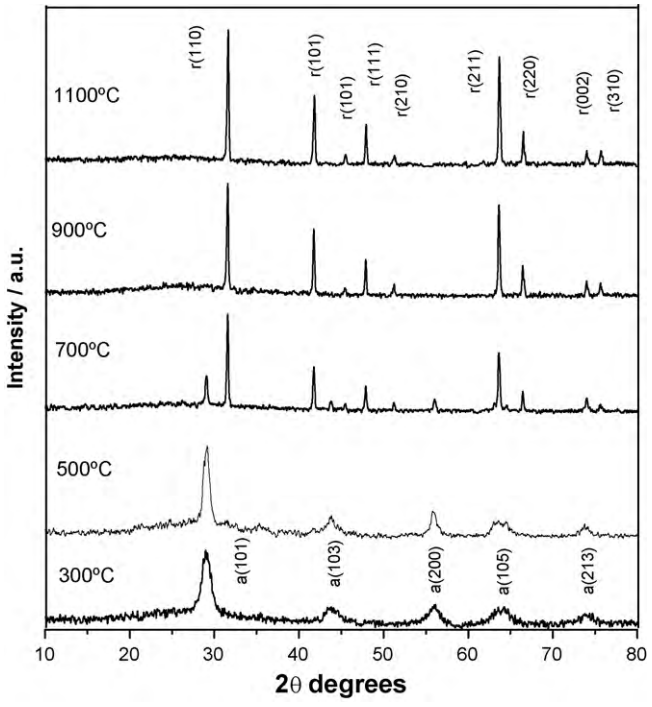

Fig. 5. X-ray diffraction patterns of TiO_2 nanoparticles heated at the indicated temperatures (a = anatase and r = rutile).

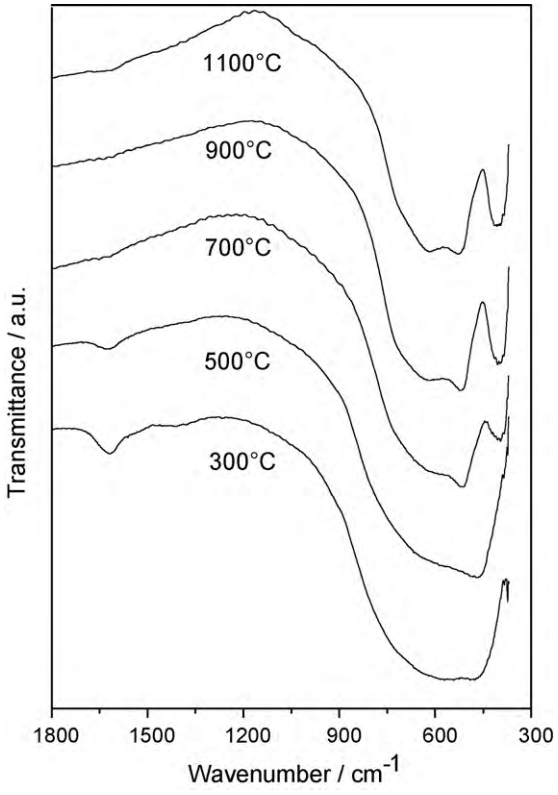

Fig. 6. Infrared spectra of TiO_2 nanoparticles heated at the indicated temperatures.

about 17–30 nm (measured by XRD and BET method). SEM image inset in Fig. 2c confirms this comment.

The sample heated at 700 °C shows an isotherm with small hysteresis loop without saturation, which is associated to meso- to macroporous materials (Fig. 2d). The specific surface area decreases to 9 $m^2 g^{-1}$ in this temperature, the amount of mesopores decreases and the macropores are characteristic of interstitial spaces between the particles. Fig. 3d shows a large pore size distribution obtained by the BJH method that reaches since mesopores until macropores. XRD analysis shows that the anatase–rutile phase transition occurs around this temperature, and they coexist in a ratio of 26% of anatase and 74% of rutile. This result is corroborated by FTIR analysis, where the large band shown by samples heated at 300 and 500 °C deconvolute into 665, 524, and 396 cm^{-1} bands. The 665 cm^{-1} mode is associated to vibration of TiO_6 octahedra of rutile TiO_2 tetragonal structure [27]. This band is shifted to 652 and 646 cm^{-1} at 900 and 1100 °C, respectively. This variation to shorter wavenumbers is explained by densification of the sample, according to porosity reduction. The SEM images confirm this result, where the secondary particles decrease and change to form the rutile phase. TGA–DTA results also show the broad event of anatase–rutile phase transition between 650 and 800 °C.

The samples heated at 900 and 1100 °C show isotherms type III (BDDT [21] classification), which characterize non-porous materials, confirmed by the SEM images (inset in Fig. 2e and f). The isotherms show that the desorption process occurs with more facility than the adsorption process (Fig. 2e and f), evidencing weak adsorption forces. The pore size distribution of the samples heated at 900 and 1100 °C was not shown in Fig. 3 due to their non-porous character, where the BJH model is not suitable. The sample heated at 1100 °C shows the lower adsorption heat and *C* constant. The diffraction peaks of these samples are related only to rutile phase, and the narrow and intense peaks are due to the largest crystallite size and crystallinity. SEM images show particle heterogeneous, spherical and elongated, with large particle size distribution. The average particle size of 380 and 690 nm to 900 and 1100 °C samples, respectively, coincide with that obtained by adsorption gas results. The FTIR bands are more defined in these temperatures than in others, confirming the presence of rutile phase with submicrometer size, also confirmed by Scherrer equation and BET method.

No samples showed photocatalytic activity and formation of free radicals during the UV irradiation, whose result is suitable for solar protection applications. The P-25 sample used to comparison showed photocatalytic activity to degrade the Drimaren red dye completely in 200 min.

Fig. 7 shows the absorption UV–vis spectra of the TiO_2 samples and the P-25 Degussa powder, used as standard. The sample heated at 300 °C has ultraviolet absorption higher than other TiO_2 powders, which do not exhibit good performance. The spectrum of this sample is similar to the P-25 ones, showing lower values in UV-A region (about 10%) and higher values in UV-B (25%) and visible regions. The high UV absorption of the powder heated at 300 °C is related to its particle size and irregular pores distribution [14], as reported by

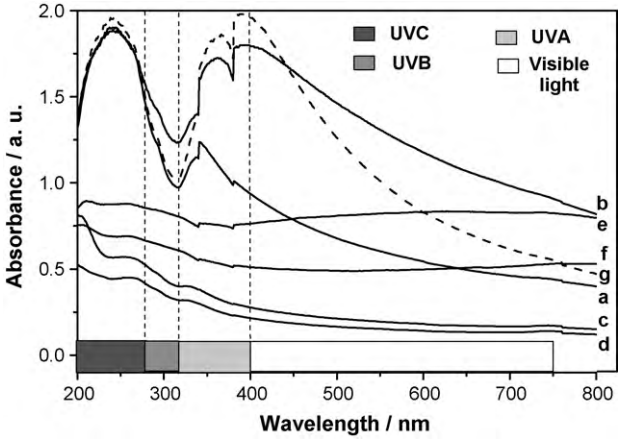

Fig. 7. Spectral absorbance of aqueous solution prepared with TiO_2 particles heated at (a) 200 °C, (b) 300 °C, (c) 500 °C, (d) 700 °C, (e) 900 °C, (f) 1100 °C and (g) P-25 Degussa.

gas adsorption technique. Popov et al. [13,14] also showed that the UV-B radiation can produce manifestation of skin erythema that are associated to increasing probability of DNA damages.

Therefore, as the TiO_2 heated at 300 °C is photostable, is easily dispersed, its dispersion has transparent character (high absorption in the visible – low reflectance), it has potentiality to be used in solar protection applications in sunscreen formulations and personal care products.

4. Conclusions

This study showed a high dependence between the heating temperature and the textural, structural, and morphological properties of TiO_2 synthesized by precipitation and thermal decomposition of the titanium alkoxide. The specific surface area and the porosity decreased systematically with the increase in heating temperature, evidencing the sample densification and the consequent increase in the average particle size. The results also showed that the amorphous TiO_2 nanoparticles crystallized to anatase nanophase below 300 °C and a diffuse phase transition for anatase to rutile occurred between 570 and 800 °C. TiO_2 nanoparticle heated at 300 °C showed potential application in solar protection.

Acknowledgements

This work was supported by Brazilian funding agencies CNPq and FAPEMIG, and by Petrobrás.

References

[1] K.K. Sahu, T.C. Alex, D. Mishra, A. Agrawal, An overview on the production of pigment grade titania from titania rich-slag, Waste Management and Research 24 (2006) 74–79.
[2] D.S. Hinczewskia, M. Hinczewskib, F.Z. Tepehana, G.G. Tepehan, Optical filters from SiO_2 and TiO_2 multi-layers using sol–gel spin coating method, Solar Energy Materials and Solar Cells 87 (2005) 181–196.
[3] G.S. Vicente, A. Morales, M.T. Gutierrez, Preparation and characterization of sol–gel TiO_2 antireflective coatings for silicon, Thin Solid Films 391 (1) (2001) 133–137.

[4] C. Garzella, E. Comini, E. Tempesti, C. Frigeri, G. Sberveglieri, TiO_2 thin films by a novel sol–gel processing for gas sensor applications, Sensors and Actuators B 68 (2000) 189–196.
[5] A.J. Maira, K.L. Yeung, C.Y. Lee, P.L. Yue, C.K. Chan, Size effects in gas-phase photo-oxidation of trichloroethylene using nanometer-sized TiO_2 catalysts, Journal of Catalysis 192 (2000) 185–196.
[6] T. Matsunaga, R. Tomoda, T. Nakajima, N. Nakamura, T. Komine, Continuous-sterilization system that uses photosemiconductor powders, Applied and Environmental Microbiology 54 (6) (1988) 1330–1333.
[7] J.-Y. Zhang, I.W. Boyd, B.J. O'Sullivan, P.K. Hurley, P.V. Kelly, J.-P. Senateur, Nanocrystalline TiO_2 films studied by optical, XRD and FTIR spectroscopy, Journal of Non-Crystalline Solids 303 (1) (2002) 134–138.
[8] L. Zhao, Y. Yu, L. Song, X. Hu, A. Larbot, Nanostructured titania film for photocatalysis, Applied Surface Science 239 (3–4) (2005) 285–291.
[9] J. Yu, M. Zhou, B. Cheng, H. Yu, X. Zhao, Ultrasonic preparation of mesoporous titanium dioxide nanocrystalline photocatalysts and evaluation of photocatalytic activity, Journal of Molecular Catalysis A: Chemical 227 (2005) 75–80.
[10] D. Bersani, P.P. Lottici, X.Z. Ding, Phonon confinement effects in the Raman scattering by TiO_2 nanocrystals, Applied Physics Letters 72 (1) (1998) 73–76.
[11] D. Bersani, P.P. Lottici, T. Lopez, X.Z. Ding, A Raman scattering study of $PbTiO_3$ and TiO_2 obtained by sol–gel, Journal of Sol–Gel Science and Technology 13 (1998) 849–853.
[12] J. Wang, B. Guo, X. Zhang, Z. Zhang, J. Han, J. Wu, Sonocatalytic degradation of methyl orange in the presence of TiO_2 catalysts and catalytic activity comparison of rutile and anatase, Ultrasonics Sonochemistry 12 (5) (2005) 331–337.
[13] A.P. Popov, A.V. Priezzhev, J. Lademann, R. Myllyla, TiO_2 nanoparticles as an effective UV-B radiation skin-protective compound in sunscreens, Journal of Physics D: Applied Physics 38 (2005) 2564–2570.
[14] A. Fourtanier, F. Bernerd, C. Bouillon, L. Marrot, D. Moyal, S. Seite, Protection of skin biological targets by different types of sunscreens, Photodermatology, Photoimmunology and Photomedicine 22 (1) (2006) 22–32.
[15] A.P. Popov, S. Haag, M. Meinke, J. Lademann, A. Priezzhev, R. Myllyla, Effect of size of TiO_2 nanoparticles applied to glass slide and porcine skin on generation of free radicals under ultraviolet irradiation, Journal of Biomedical Optics 14 (2) (2009).
[16] A. Bojinova, R. Kralchevska, I. Poulios, C. Dushkin, Anatase/rutile TiO_2 composites: influence of the mixing ratio on the photocatalytic degradation of Malachite Green and Orange II in slurry, Materials Chemistry and Physics 106 (2007) 187–192.
[17] T. Ohno, K. Sarukawa, K. Tokieda, M. Matsumura, Morphology of a TiO_2 photocatalyst (Degussa, P-25) consisting of anatase and rutile crystalline phases, Journal of Catalysis 203 (1) (2001) 82–86.
[18] S. Kim, S.H. Ehrman, Photocatalytic activity of a surface-modified anatase and rutile titania nanoparticle mixture, Journal of Colloid and Interface Science 338 (1) (2009) 304–307.
[19] B.D. Cullit, Elements of X-ray Diffraction, 2nd ed., Addison-Welley Publishing Company, USA, 1987.
[20] R.A. Spurr, H. Myers, Quantitative analysis of anatase–rutile mixtures with an X-ray diffractometer, Analytical Chemistry 29 (5) (1957) 760–762.
[21] S.J. Gregg, K.S.W. Sing, Adsorption, Surface Area and Porosity, 2nd ed., John Wiley, NY, 1992.
[22] L.I. Bekkerman, I.P. Dobrovolskii, A.A. Ivakin, Effect of composition of titanium(IV) solutions and precipitation conditions on solid-phase structure, Russian Journal of Inorganic Chemistry 21 (2) (1976) 418–422.
[23] W.F. Sullivan, S.S. Cole, Thermal chemistry of colloidal titanium dioxide, Journal of the American Ceramic Society 42 (3) (1959) 127–133.
[24] H. Richter, Z.P. Wang, L. Ley, The one phonon Raman spectrum in microcrystalline silicon, Solid State Communications 39 (5) (1981) 625–629.
[25] W. Guo, Z. Lin, X. Wang, G. Song, Sonochemical synthesis of nanocrystalline TiO_2 by hydrolysis of titanium alkoxides, Microelectronic Engineering 66 (1–4) (2003) 95–101.
[26] H. Jensen, A. Soloviev, Z. Li, E.G. Sogaard, XPS and FTIR investigation of the surface properties of different prepared titania nano-powders, Applied Surface Science 246 (1–3) (2005) 239–249.
[27] T. Ivanova, A. Harizanova, Characterization of TiO_2 and TiO_2–MnO oxides prepared by sol–gel method, Solid State Ionics 138 (2001) 227–232.
[28] J. Yang, J.M.F. Ferreira, W. Weng, Y. Tang, Sol–gel preparation and electrorheological activity of SiO_2–TiO_2 composite powders, Journal of Colloid and Interface Science 195 (1997) 59–65.
[29] N. Kaliwoh, J.-Y. Zhang, I.W. Boyd, Titanium dioxide films prepared by photo-induced sol–gel processing using 172 nm excimer lamps, Surface and Coatings Technology 125 (2000) 424–427.